

Ricardo R. Ambriz
David Jaramillo
Gabriel Plascencia
Moussa Nait Abdelaziz *Editors*

Proceedings of the 17th International Conference on New Trends in Fatigue and Fracture

 Springer

**Proceedings of the 17th International Conference
on New Trends in Fatigue and Fracture**

Ricardo R. Ambriz · David Jaramillo
Gabriel Plascencia · Moussa Nait Abdelaziz
Editors

Proceedings of the 17th International Conference on New Trends in Fatigue and Fracture

Editors

Ricardo R. Ambriz
CIITEC-Instituto Politécnico Nacional
Mexico City
Mexico

Gabriel Plascencia
CIITEC-Instituto Politécnico Nacional
Mexico City
Mexico

David Jaramillo
CIITEC-Instituto Politécnico Nacional
Mexico City
Mexico

Moussa Nait Abdelaziz
Polytech' Lille
Université des Sciences et
Technologies de Lille
Villeneuve-d'Ascq
France

ISBN 978-3-319-70364-0 ISBN 978-3-319-70365-7 (eBook)
<https://doi.org/10.1007/978-3-319-70365-7>

Library of Congress Control Number: 2017959154

© Springer International Publishing AG 2018

This work is subject to copyright. All rights are reserved by the Publisher, whether the whole or part of the material is concerned, specifically the rights of translation, reprinting, reuse of illustrations, recitation, broadcasting, reproduction on microfilms or in any other physical way, and transmission or information storage and retrieval, electronic adaptation, computer software, or by similar or dissimilar methodology now known or hereafter developed.

The use of general descriptive names, registered names, trademarks, service marks, etc. in this publication does not imply, even in the absence of a specific statement, that such names are exempt from the relevant protective laws and regulations and therefore free for general use.

The publisher, the authors and the editors are safe to assume that the advice and information in this book are believed to be true and accurate at the date of publication. Neither the publisher nor the authors or the editors give a warranty, express or implied, with respect to the material contained herein or for any errors or omissions that may have been made. The publisher remains neutral with regard to jurisdictional claims in published maps and institutional affiliations.

Printed on acid-free paper

This Springer imprint is published by Springer Nature
The registered company is Springer International Publishing AG
The registered company address is: Gewerbestrasse 11, 6330 Cham, Switzerland

Contents

Theoretical and Experimental Analysis of the Energy Dissipation at Fatigue Crack Tip Under Cyclic Loading with Constant Stress Intensity Factor	1
O. Plekhov, A. Vshivkov and A. Iziumova	
A Study of Progressive Milling Technology on Surface Topography and Fatigue Properties of the High Strength Aluminum Alloy 7475-T7351	7
Miroslav Piska, Petra Ohnistova, Jana Hornikova and Charles Hervoches	
Study and Design of a New Range of Composite Based Shock Absorbers for the Automotive Sector	19
J. Niez, M. Ben Amara, J. Capelle, V. Bouchart and P. Chevrier	
A New High-Cycle Fatigue Criterion Based on a Self-consistent Scheme for Hard Metals Under Non-proportional Loading	29
Kékéli Amouzou and Eric Charkaluk	
Characterization and Evaluation of a Railway Wheel Steel in the HCF and VHCF Regimes	41
Henrique Soares, Pedro Costa, Mário Vieira, Manuel Freitas and Luís Reis	
High-Temperature Low Cycle Fatigue Resistance of Inconel 713LC Coated with Novel Thermal Barrier Coating	49
Ivo Šulák, Karel Obrtlík, Ladislav Čelko, David Jech and Pavel Gejdoš	
The Effect of Pearlite Banding on the Mechanical Anisotropy of Low Carbon Steel	57
M. Beltrán, J. L. González, D. I. Rivas, Felipe Hernández and Héctor Dorantes	

Analysis of Mechanical Behavior of the Underlying Soft Tissue to Ischial Tuberosities Using Finite Element Method	67
Diana Alicia Gayol-Mérida, Víctor Manuel Araujo-Monsalvo, José de Jesús Silva-Lomelí, Víctor Manuel Domínguez-Hernández, Marcos Martínez-Cruz, Elisa Martínez-Coría, Martín Luna-Méndez and Ayleneid Alemán-Pérez	
Study of the Endurance Limit of AA7075 Aluminum Produced by High-Pressure Vacuum Die Casting Analyzed by Classical Whöler Curve	75
David Levasseur, Jimmy Simard, Francis Breton and Lotfi Toubal	
Life Prediction of a Mono Contact Aluminum/Steel at Constant and Variable Amplitudes Loading in Fretting Fatigue Configuration	85
A. Belloula, A. Amrouche and M. Nait-Abdelaziz	
Influence of Microstructure on Fatigue Crack Formation and Growth in a Low-Carbon Steel	91
Donka Angelova, Rozina Yordanova and Svetla Yankova	
Determination of the Region of Stabilization of Low-Cycle Fatigue HSLE Steel from Test Data	101
Bojana Aleksić, Vujadin Aleksić, Abubakr Hemer, Ljubica Milović and Aleksandar Grbović	
Study of a Stud Bolt Wrench Failure Due to an Inadequate Heat Treatment.	113
Sandra L. Rodriguez-Reyna, Francisco G. Perez-Gutierrez, J. Luis Hernández-Rivera, Jorge Zaragoza-Siqueiros and Christian J. Garcia-Lopez	
Multiaxial Fatigue of Rubbers: Comparative Study Between Predictive Tools	123
G. Ayoub, M. Naït Abdelaziz and F. Zaïri	
Laboratory Study of Fatigue in Water Conveying HDPE and PVC Pipes Subject to Extreme Hydraulic Transient Pressures	129
René Autrique Ruiz and Eduardo Antonio Rodal Canales	
Probabilistic Assessment of Nuclear Piping Integrity by Considering Environmental Fatigue and Stress Corrosion Cracking	139
Seung Hyun Kim, Md Nasimul Goni and Yoon-Suk Chang	
The Inspections, Standards and Repairing Methods for Pipeline with Composite: A Review and Case Study	147
M. Hadj Meliani, O. Bouledroua, Z. Azari, A. Sorour, N. Merah and G. Pluvinage	

Effect of Microstructure on Tension, Charpy and DWTT Properties on Two API X70 Plates	157
Fernando Guzmán, Moisés Hinojosa and Eduardo Frias	
Fatigue Analysis in a Bellow Expansion Joint Installed a Heat Exchanger	165
I. Villagómez, J. L. González, J. J. Trujillo and D. Rivas	
Failure Analysis of Stress Corrosion Cracking of a Ball Valve in Service	173
I. Mortera, J. L. González, A. Casarrubias and D. Rivas	
Assessment of Danger Due to Cracks in Structural Elements of Different Shapes and Geometry	181
Orest Bilyy	
Formation of Preferential Paths in Cracked Hele-Shaw Cells by Water Injection—An Experimental Study	189
S. de Santiago, I. V. Lijanova, C. O. Olivares-Xometl and N. V. Likhanova	
Smith Watson and Topper Model in the Determination of the Fatigue Life of an Automotive Steel	197
F. F. Curiel, R. R. Ambriz, M. A. García, M. C. Ramírez and S. García	
Influence of Weld Parameters and Filler-Wire on Fatigue Behavior of MIG-Welded Al-5083 Alloy	209
Vidit Gaur, Manabu Enoki, Toshiya Okada and Syohei Yomogida	
Mechanical Evaluation of IN718-AL6XN Dissimilar Weldment	215
R. Cortés, R. R. Ambriz, V. H. López, E. R. Barragán, A. Ruiz and D. Jaramillo	
Fatigue Life of Resistance Spot Welding on Dual-Phase Steels	225
J. H. Ordoñez Lara, R. R. Ambriz, C. García, G. Plascencia and D. Jaramillo	
Failure Analysis by Hot Cracking Root HAZ in Welding SMAW Type	237
M. Arzola, J. L. González, S. J. García, D. I. Rivas and E. Sandoval	
Effect of Electromagnetic Field on the Microstructure and Mechanical Properties of the Dissimilar 2205/316L Welded Joint	247
S. L. Hernández-Trujillo, V. H. López-Morelos, R. García-Hernández, M. A. García-Rentería, A. Ruiz-Marines and J. A. Verduzco-Martínez	
Heat Input Effect on the Mechanical Properties of Inconel 718 Gas Tungsten Arc Welds	255
N. K. Rodríguez, E. R. Barragán, I. V. Lijanova, R. Cortés, R. R. Ambriz, C. Méndez and D. Jaramillo	

A Case Study of Corrosion Fatigue in Aluminium	
Casing Bolt Holes	263
Siew Fong Choy	
Study of the Modal Effect of 1045 Steel Pre-stressed Beams Subjected to Residual Stress	269
Erasto Vergara Hernández, Brenda Carolina Pérez Millán, Juan Manuel Sandoval Pineda and Luis Armando Flores Herrera	
Experimental Analysis of Fatigue Cracks Emanating from Corner Notches in the Presence of Variable Residual Stress Fields	273
J. L. Cuevas, C. Garcia, A. Amrouche, R. R. Ambriz and D. Jaramillo	
Fatigue Crack Initiation and Growth on Welded Joints of 2205 Duplex Alloy: The Effect of Electromagnetic Interaction During Welding	281
J. Rosado-Carrasco, J. González-Sánchez, V. H. López-Morelos and G. R. Domínguez	
Nondestructive Monitoring of Rail Surface Damage Via Barkhausen Noise Technique	287
M. Neslušán, K. Zgútová, I. Maňková, P. Kejzlar and J. Čapek	
Failure Analysis of Stress Corrosion Cracking of Two Tees in a Pressurized Drainage System	299
D. Rivas, J. L. González, A. Casarrubias and M. Beltran	
Fatigue Life Extension of 2205 Duplex Stainless Steel by Laser Shock Processing: Simulation and Experimentation	307
V. Granados-Alejo, C. A. Vázquez-Jiménez, C. Rubio-González and G. Gómez-Rosas	
Fracture Toughness of Fiber Metal Laminates Through the Concepts of Stiffness and Strain-Intensity-Factor	313
Jesús Gerardo Martínez Figueroa and Perla Itzel Alcántara Llanas	
Uncertainty Quantification of Fatigue Life Prediction in Welded Structures Using Microstructure-Based Simulations	329
Takayuki Shiraiwa, Fabien Briffod and Manabu Enoki	
Prediction of Fatigue Life Induced by Defects Considering Crack Initiation	335
Ryota Sakaguchi, Takayuki Shiraiwa and Manabu Enoki	
Peridynamic Modeling of Cracking in Ceramic Matrix Composites	341
Yile Hu, Erdogan Madenci and Nam Phan	
Evaluation of Stress Intensity Factors (SIFs) Using Extended Finite Element Method (XFEM)	355
Bojana Aleksić, Aleksandar Grbović, Abubakr Hemer, Ljubica Milović and Vujadin Aleksić	

Evaluation of Stress Intensity Factors (SIFs) Using Extended Finite Element Method (XFEM)

Bojana Aleksić, Aleksandar Grbović, Abubakr Hemer,
Ljubica Milović and Vujadin Aleksić

Introduction

Finite element analysis is a numerical method that makes it possible to solve very complex problems. This method uses physical discretization of domains, so that complex spatial structures in the calculations are considered as discrete systems. The development of engineering structures presupposes the existence of very precise calculations, which provide optimum weight, load capacity and structural safety. The idea of division of domains into a number of subdomains is very old, but the intensive development of the method of finite elements is only foreboded in the middle of the twentieth century.

The finite element is defined by its shape, number and position of the adjacent nodes. Calculation by the finite element method begins with discretization consisting of the selection of interpolation functions (element shape functions) as well as the selection of refinement of the finite element mesh. Interpolation functions (shape functions) approximately determine the true field of variables at any point within an element, interpolating the values of the variables in the nodes of that

B. Aleksić (✉)

Innovation Centre of Faculty of Technology and Metallurgy,
Karnegijeva 4, 11120 Belgrade, Serbia
e-mail: baleksic@tmf.bg.ac.rs

A. Grbović

Faculty of Mechanical Engineering, University of Belgrade,
Kraljice Marije 16, 11120 Belgrade, Serbia

A. Hemer · L. Milović

Faculty of Technology and Metallurgy, University of Belgrade,
Karnegijeva 4, 11120 Belgrade, Serbia

V. Aleksić

Institute for Testing Materials-IMS Institute, Bulevar Vojvode Mišića 43,
11000 Belgrade, Serbia

element. By solving formed differential equations for the finite element mesh, the required magnitudes are calculated (displacement, strain, internal forces, stress) [1].

The finite element method is very often used to calculate the structures with the cracks-pre-cracked structures.

In addition to the classical finite elements, there is an extended Finite Element Method (XFEM) that will be discussed in this paper. The basic characteristic of XFEM is that it allows the modeling of a discontinuous physical field independently of the generated network of finite elements. Unlike the classic finite element method, where the cracks growth process requires the successive generation of a network to be able to monitor the increasing geometric discontinuity, the XFEM does not require a comfortable mapping between the network and the discontinuity geometry.

In this paper, a simulation of the central-crack propagation was conducted using the example of a finite-dimension plate, and a comparative overview of the results obtained using Abaqus and the FRANC2D/L software presented.

3D Simulation of the Central-Crack Propagation on the Finite-Dimension Plate

It is a plate of constant thickness ($t = 25.4$ mm) and slightly larger dimensions (508×254 mm), but with a central initial crack 254 mm long (Fig. 1). The model of the central-crack plate is defined in the CATIA v5 [2] software, from where it was exported to Abaqus. The initial crack in CATIA v5 is defined as a surface without thickness, while Abaqus defines the characteristics of the material

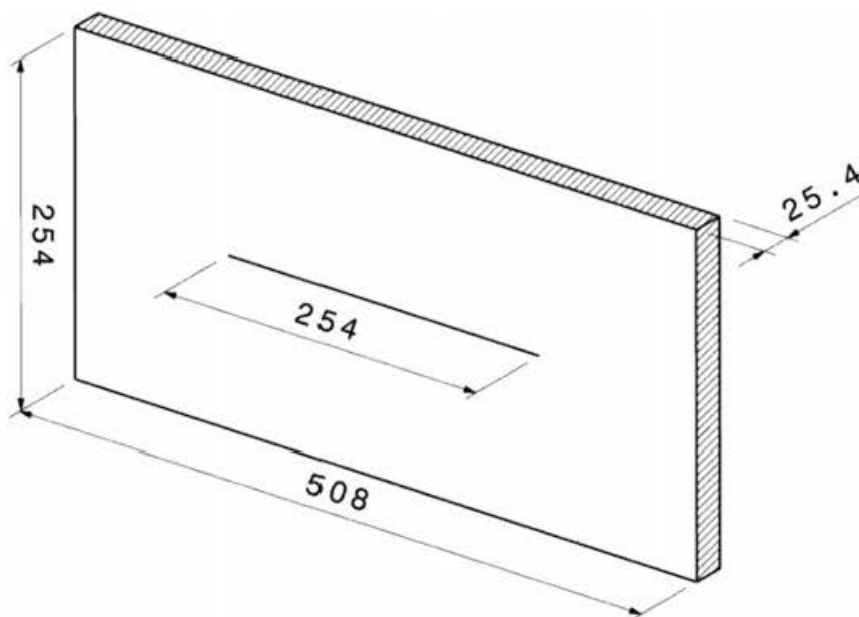


Fig. 1 Dimensions of the plate with central crack, used for 3D simulation of propagation

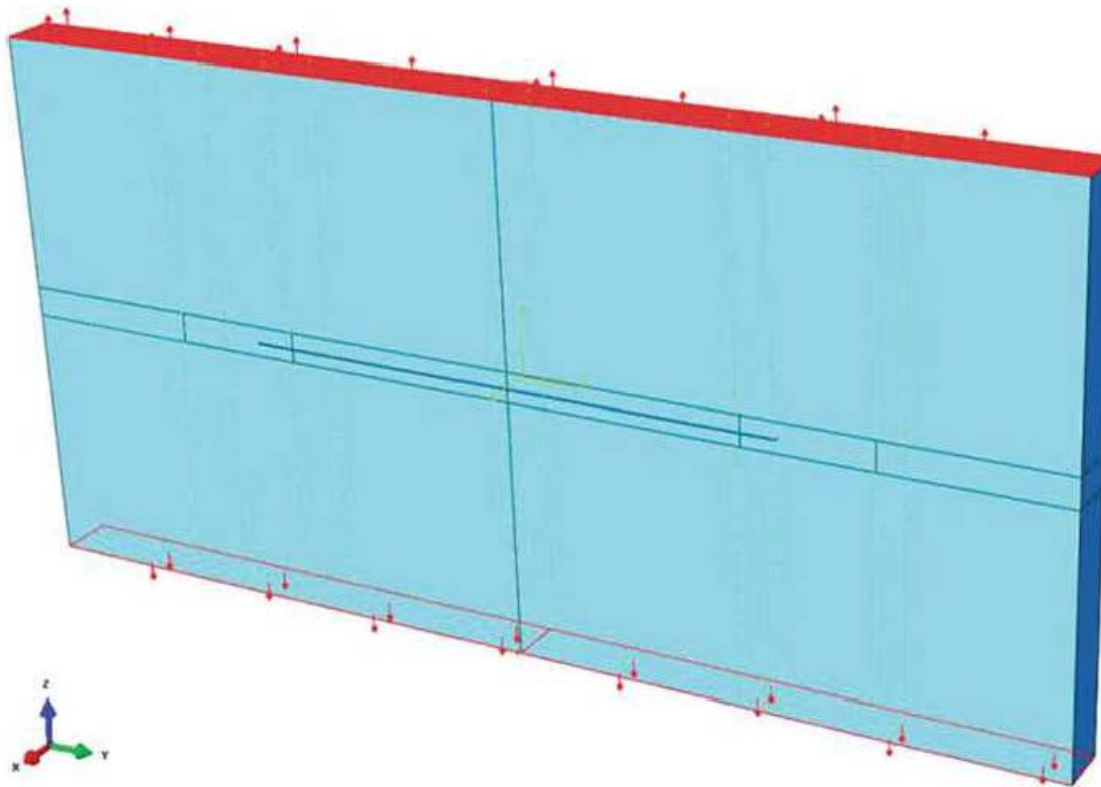


Fig. 2 Loading of the 508 × 254 mm plate with central crack (Abaqus model)

(steel with Young's modulus of elasticity 206,800 MPa and Poisson's coefficient 0.3), uniform tensile stress (value 6.89 kPa) on the upper and lower surface of the plate and the corresponding boundary conditions (Fig. 2).

In Abaqus, two meshes of finite elements—mesh with hexahedra (Fig. 3) and mesh with tetrahedra (Fig. 4) are defined to compare the results obtained for different types of elements. In Figs. 3 and 4 it can be seen that in the areas through which the crack propagates a very “thick” mesh is generated, in order to increase the accuracy of the values obtained by calculation using a larger number of nodes. The Figs show the outlook of the meshes that gave the best results and that came after several iterations through which the meshes were gradually improved. The final mesh consisting of hexahedral elements had 128,190 elements, while the tetrahedral mesh consisted of 917,880 elements.

Figures 5 and 6 show the values of von Mises stress around the crack on the hexahedral mesh after the first step of the calculation (crack opening displacement). The maximum value of the stress adjacent to the crack tip was 0.703 MPa, which is quite a low value, but it should not be surprising since the applied tensile stress at the ends of the plate was only 0.00689 MPa.

Such a low stress value was adopted to study the variation in the value of the stress intensity factor in the case of low external stress, as well as to compare the value of the stress intensity after the crack opening displacement with the value given in the literature [3], which was also obtained by the extended finite element

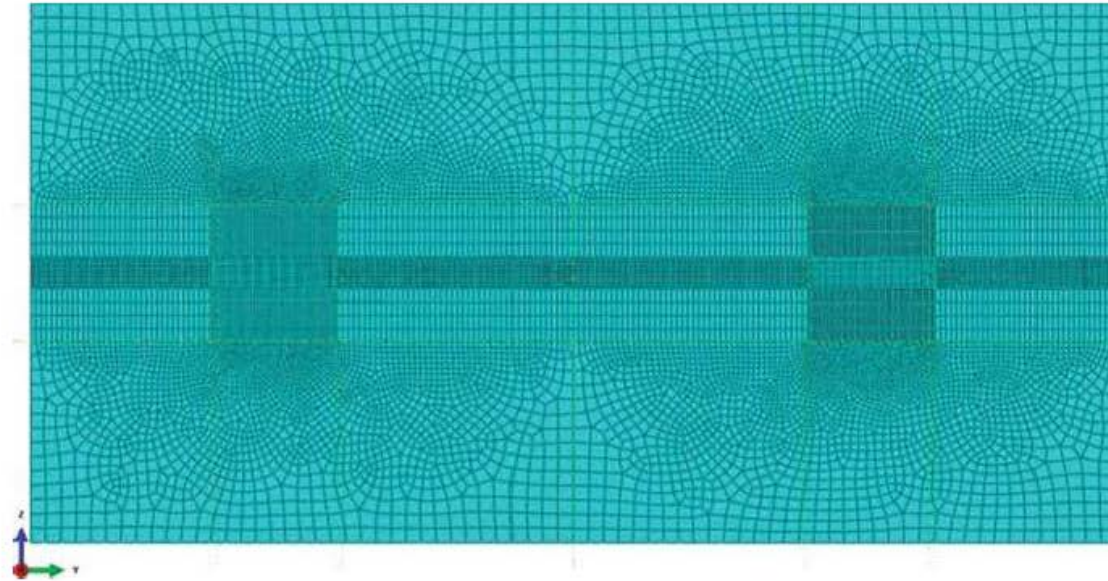


Fig. 3 The finite-element mesh of the model of pre-cracked 508 × 254 mm plate (hexahedral elements)

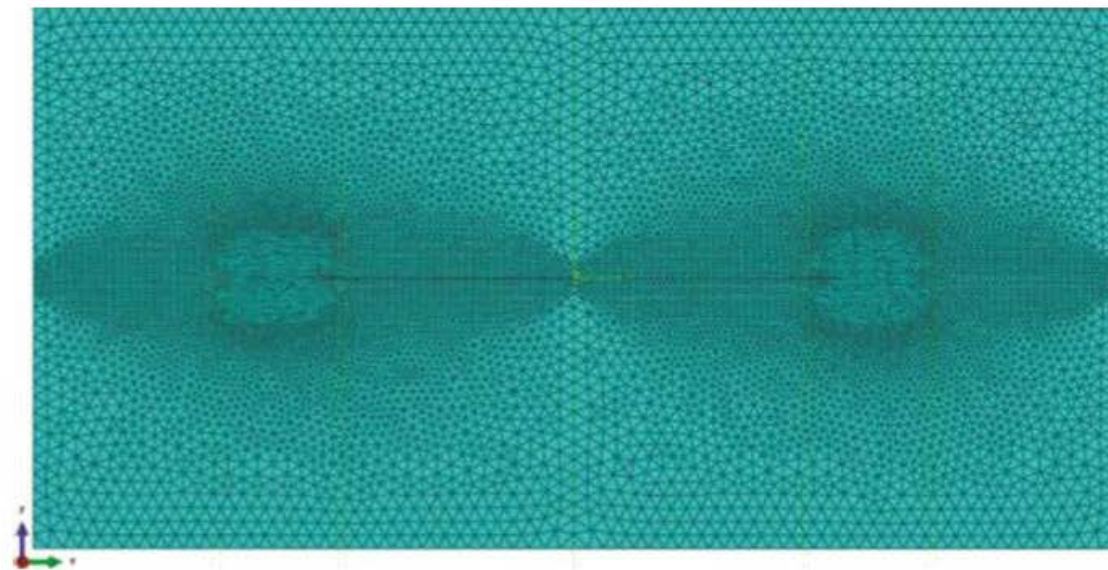


Fig. 4 Finite-element mesh of the model of pre-cracked 508 × 254 mm plate (tetrahedral elements)

method, but in 2D analysis. Otherwise, the value of the K_I intensity factor in the case of the plate with central crack can be determined by the formula:

$$K_I^{(\text{teor.})} = \sigma \cdot f\left(\frac{a}{W}, \frac{L}{W}\right) \cdot \sqrt{\pi a} \quad (1)$$

where factor of correction $f\left(\frac{a}{W}, \frac{L}{W}\right)$ is determined from the tables of the values that also can be found in literature [4]. In this case $\frac{a}{W} = \frac{254}{508} = 0.5$, $\frac{L}{W} = \frac{254}{508} = 0.5$, then



Fig. 5 Stress state (von Mises) of the plate after crack opening displacement (hexahedral elements)

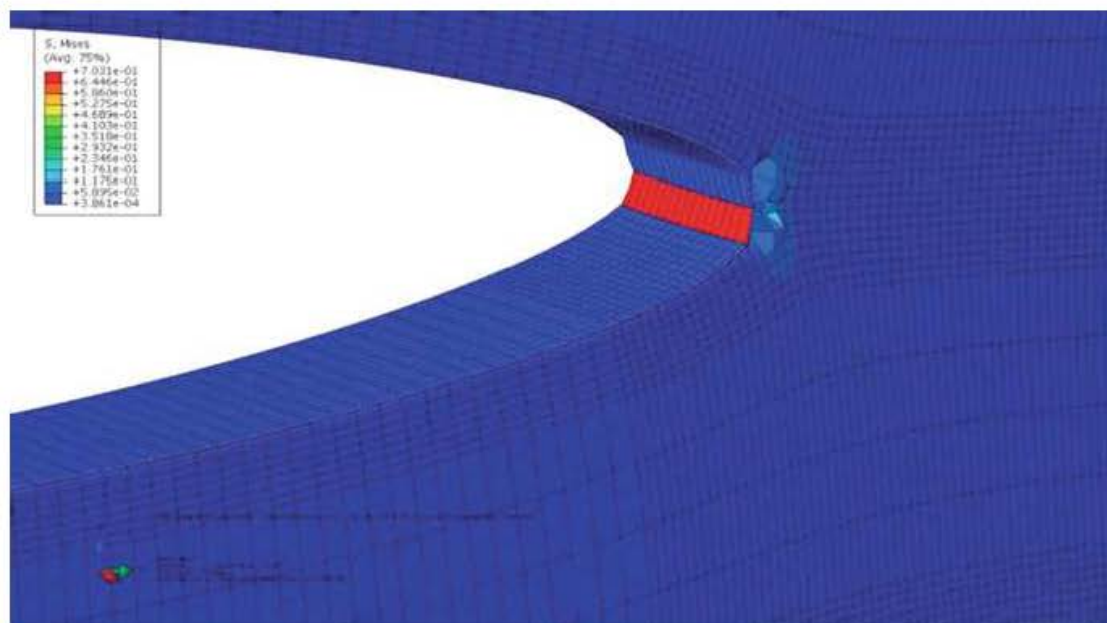


Fig. 6 Stress state (von Mises) of the plate after crack opening displacement (hexahedral elements —magnified presentation)

$f(0.5, 0.5) \approx 1.9$, so that theoretical value of K_I is: $K_I^{(theor.)} = 261.08 \text{ KPa mm}^{0.5} = 0.26108 \text{ MPa mm}^{0.5}$

The values of K_I obtained from the 2D analysis ranged from $239.08 \text{ KPa mm}^{0.5}$ to as much as $405.99 \text{ KPa mm}^{0.5}$, and were obtained for different size of the

integration domain (relative to the length of the crack) and using different methods (classical FEM and XFEM were used) [5]. The XFEM gave far better predictions, since the average deviations from the theoretical value (for different sizes of the integration domain) amounted to only 1%. The average value of K_I , obtained after the crack opening displacement on the 3D model with hexahedral elements (Figs. 5 and 6), was $288.3 \text{ KPa mm}^{0.5}$, which is about 10% above the theoretical value and the values from [3]. However, this is the mean value obtained based on 64 stress intensity factors calculated at the same number of points on the front of the 3D crack, while the theoretical value and the value from the 2D analysis using FEM were calculated at only one point of the crack tip. As for the plate with tetrahedral elements, a slightly lower value of K_I ($281.1 \text{ KPa mm}^{0.5}$) was obtained.

Figures 7 and 8 show the values of von Mises stress around the crack on the tetrahedral mesh after the first step. The maximum stress (1.032 MPa) is slightly higher than that of the plate with hexahedral elements.

In the available literature, however, the values of the stress intensity factor obtained by applying the XFEM to further crack propagation after the “opening” of the initial damage 254 mm-long cannot be found. In the NASGRO base of standard samples, there is an example of a plate with a crack in the middle, but the values of the stress intensity factor obtained in the NASGRO v4 software cannot be used to verify the solutions obtained using XFEM in Abaqus, because the NASGRO uses a plate of infinite length for a calculation.

Plate dimensions significantly affect the accuracy of the results obtained using the FEM so that, in order to verify the results, the values obtained for the 2D plate model calculated in the FRANC2D/L software had to be used here. In Figs. 9 and 10, the



Fig. 7 Stress state (von Mises) of the plate after crack opening displacement (tetrahedral elements)

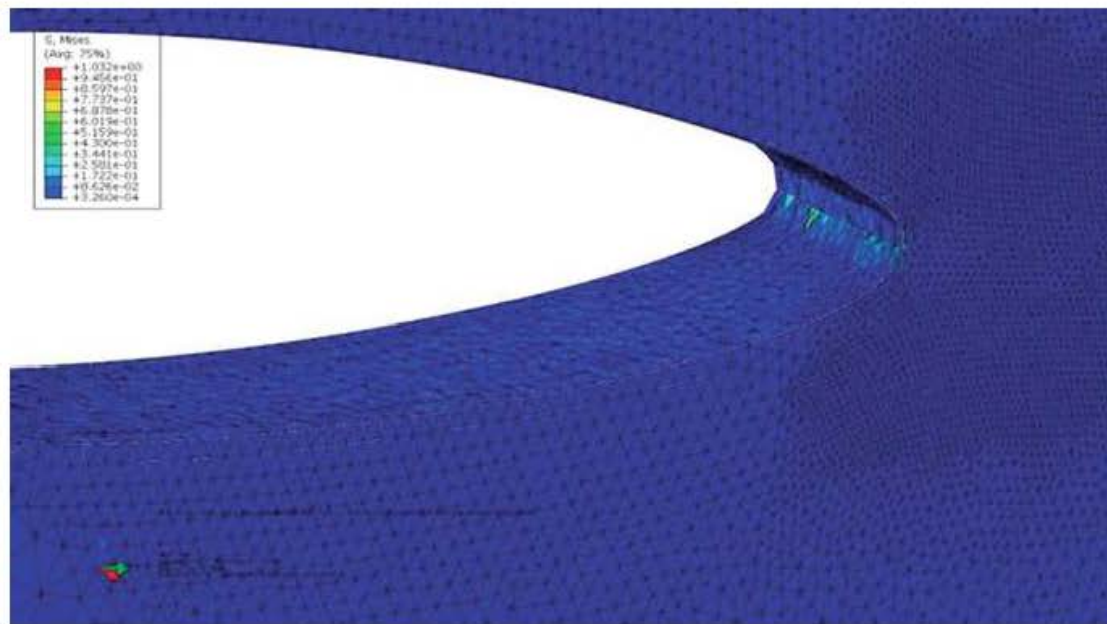


Fig. 8 Stress state (von Mises) of the plate after crack opening displacement (tetrahedral elements —magnified presentation)



Fig. 9 Stress state (von Mises) of a plate after 18 steps of crack propagation (hexahedral elements)

stress state of the plates with hexahedral and tetrahedral elements after 18 crack propagation steps is shown, while Fig. 11 shows the appearance of the mesh of the central-crack plate generated in the FRANC2D/L software.

The model in FRANC2D/L was loaded with the same tensile stress at the ends of the plate as well as the model in Abaqus, and the same boundary conditions and



Fig. 10 Stress state (von Mises) of a plate after 18 steps of crack propagation (tetrahedral elements)

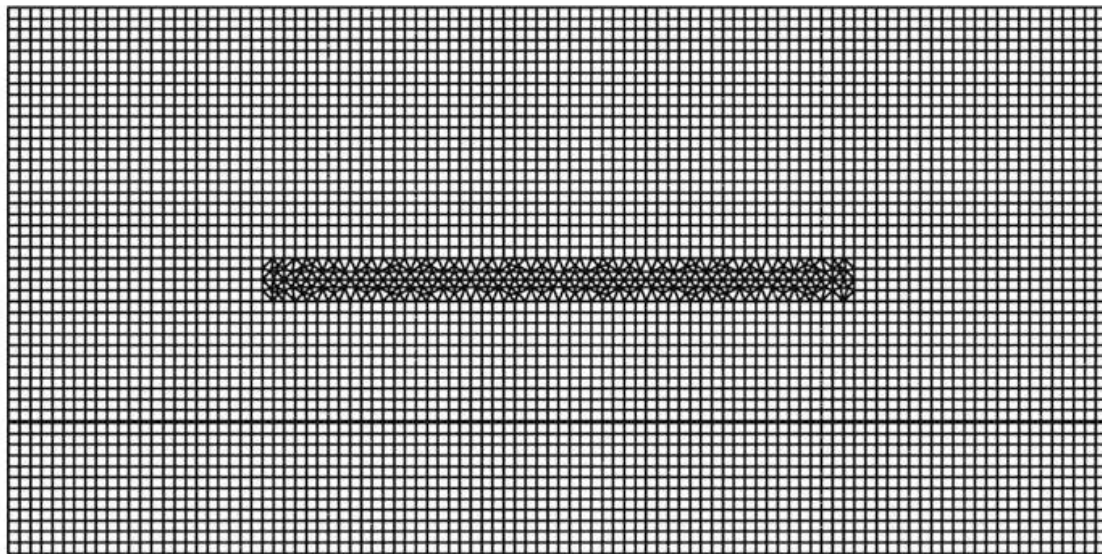


Fig. 11 The appearance of the mesh of elements of the central-crack 508×254 mm plate in the FRANC2D/L software

material characteristics were applied (plate thickness is one of them), too. The final appearance of the deformed mesh of elements in Fig. 12 confirmed that all the crack-propagation parameters were well defined, since the mesh is very similar to the deformed 3D meshes shown in Figs. 9 and 10. The crack shape shown in Fig. 12 was obtained after a 20 propagation step (crack opening displacement +19

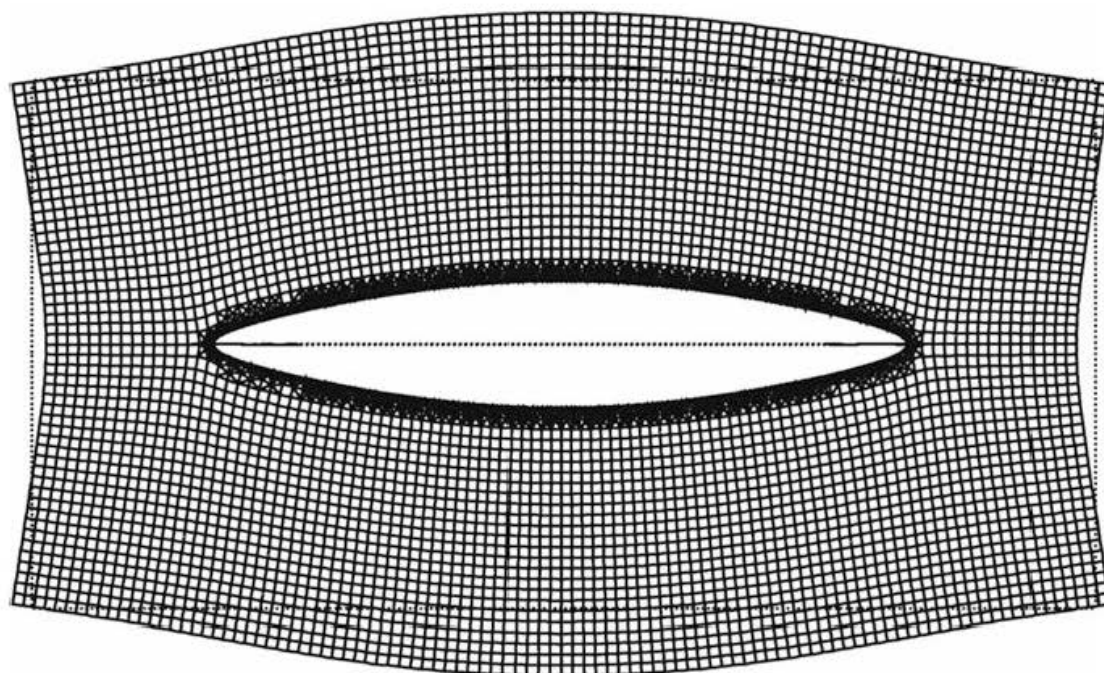


Fig. 12 The appearance of the deformed mesh of elements in the FRANC2D/L software after 20 steps of crack propagation

propagations), so that the appearance of the plate is slightly different than in Figs. 9 and 10, because in the 3D simulations 18 steps of propagation of a maximum value of 2.5 mm were carried out in both crack tips. The final crack length, therefore, was 339 mm for the 3D model, and 349 mm for the 2D. In both simulations (2D and 3D), the option for free crack propagation was used, that is, they were not “forced” to move in the plane. However, in all three cases, cracks propagated exclusively in the horizontal plane.

Table 1 gives the values of the stress intensity factor obtained by simulation of crack propagation on the plate with hexahedral elements, while the values given in Table 2 were obtained on the plate with tetrahedral elements.

What can be observed is that **the differences between the minimum and maximum values and the equivalent stress safety factor of Mode I are now significantly lower than in the first case**, which confirms the conclusion that the shape and density of the mesh have a significant effect on the accuracy of the results obtained using the extended finite element method.

In the model of the central-crack plate, it is easier to make a quality mesh of elements since it has no hole that is the source of the stress concentration and around which the mesh must be carefully generated to prevent the occurrence of unrealistically high or low stress values.

The values in Table 1 show that on the mesh with hexahedrons the number of the front points in which the values of K_{ekv} and K_I were calculated was constant almost all the time and was 64 (in a few steps it was somewhat larger, 66 and 68), **and that calculated mean values of the equivalent stress intensity factor and stress intensity factor of Mode I in all steps were almost identical**. This shows

Table 1 The value of the equivalent stress intensity factor and stress intensity factor Mode I in the case of the model with hexahedral elements

Step	Length of the crack (mm)	Number of front points	Hexahedral elements					
			The value of the equivalent stress intensity factor, K_{ekv} (MPamm ^{0.5})			Stress intensity factor Mode I, K_I (MPamm ^{0.5})		
			Max	Min	Mean values	Max	Min	Mean values
1	254	64	0.2926	0.2823	0.2884	0.2923	0.2822	0.2883
2	259	64	0.3015	0.2944	0.2981	0.3012	0.2942	0.2978
3	264	64	0.3076	0.3056	0.3069	0.3073	0.3055	0.3067
4	269	64	0.3177	0.3143	0.3159	0.3174	0.3142	0.3156
5	274	64	0.3265	0.3238	0.3252	0.3264	0.3236	0.3249
6	279	64	0.3364	0.3332	0.3346	0.3361	0.3332	0.3343
7	284	64	0.3471	0.3427	0.3448	0.3469	0.3427	0.3445
8	289	64	0.3562	0.3534	0.3657	0.3559	0.3533	0.3542
9	294	64	0.3684	0.3632	0.3755	0.3681	0.3631	0.3654
10	299	64	0.3769	0.3739	0.3879	0.3766	0.3735	0.3753
11	304	64	0.3915	0.3848	0.3879	0.3913	0.3847	0.3876
12	309	64	0.4000	0.3956	0.3982	0.3997	0.3952	0.3978
13	314	64	0.4151	0.4082	0.4114	0.4148	0.4080	0.4111
14	319	66	0.4241	0.4196	0.4224	0.4238	0.4194	0.4221
15	324	64	0.4390	0.4332	0.4363	0.4386	0.4330	0.4360
16	329	66	0.4499	0.4472	0.4482	0.4496	0.4469	0.4479
17	334	66	0.4661	0.4596	0.4629	0.4656	0.4594	0.4625
18	339	68	0.5121	0.5048	0.5087	0.5118	0.5046	0.5084

that the values of the stress intensity factors of the Modes II and III were either negligibly small or negative, that is, that these modes do not occur at all during the crack propagation. And indeed, by inspecting the files in which Abaqus kept all calculated values during the propagation step, enough arguments were found to confirm the previous conclusion.

Through the analysis of the values presented in Table 2 (case of the plate with tetrahedral elements) one can come to the same conclusion as in the case of the plate with hexahedral elements: **the difference between the mean values of the equivalent stress intensity factor and the intensity factors of Mode I is almost negligible in all steps**, indicating the absence of Modes II and III during crack propagation. Unlike the hexahedral plate, the number of the front points on the tetrahedral plate steadily increased from step to step, from 254 points (as it was at the beginning) to 339 points (as it was in the last propagation). It is assumed that this is a consequence of the very shape of the tetrahedral element through which the crack propagates, and here we can mention another fact that additionally clarifies the great difference in the number of front points: the number of finite elements on

Table 2 The value of the equivalent stress intensity factor and stress intensity factor of Mode I in the case of the model with tetrahedral elements

Step	Length of the crack (mm)	Number of front points	Tetrahedral elements					
			The value of the equivalent stress intensity factor, K_{ekv} (MPa mm ^{0.5})			Stress intensity factor Mode I, K_I (MPa mm ^{0.5})		
			Max	Min	Mean values	Max	Min	Mean values
1	254	190	0.2871	0.2711	0.2814	0.2870	0.2707	0.2811
2	259	208	0.2927	0.2844	0.2893	0.2925	0.2838	0.2890
3	264	222	0.3006	0.2946	0.2982	0.3008	0.2938	0.2980
4	269	226	0.3074	0.3045	0.3059	0.3087	0.3039	0.3056
5	274	217	0.3194	0.3110	0.3158	0.3193	0.3100	0.3155
6	279	212	0.3259	0.3215	0.3242	0.3259	0.3210	0.3240
7	284	227	0.3348	0.3291	0.3330	0.3342	0.3255	0.3324
8	289	208	0.3460	0.3382	0.3434	0.3456	0.3276	0.3420
9	294	216	0.3543	0.3500	0.3529	0.3544	0.3364	0.3515
10	299	212	0.3688	0.3596	0.3631	0.3640	0.3525	0.3602
11	304	212	0.3794	0.2701	0.3743	0.3753	0.3649	0.3721
12	309	199	0.3938	0.3814	0.3845	0.3871	0.3810	0.3831
13	314	203	0.4026	0.3934	0.3970	0.3982	0.3906	0.3955
14	319	184	0.4120	0.3960	0.4082	0.4126	0.3908	0.4069
15	324	155	0.4223	0.4136	0.4186	0.4216	0.4066	0.4167
16	329	152	0.4354	0.4246	0.4308	0.4351	0.4232	0.4301
17	334	126	0.4566	0.4453	0.4496	0.4547	0.4405	0.4476
18	339	107	0.5122	0.4951	0.5026	0.5110	0.4953	0.5025

the plate with tetrahedrons is significantly higher than the number of elements on the hexahedral plate—917,880 versus 128,190, which is a ratio of 7:1.

The graph in Fig. 13 shows that the differences in the values of the equivalent stress intensity factors obtained on the plates with these two types of elements are almost negligible, although it is evident that the values obtained on the tetrahedral plate are in all steps lower than those on the hexahedral plate. Taking into consideration the results obtained in the FRANC2D/L software as well, it is possible to draw a new diagram (Fig. 14) which shows that the values of the stress intensity factor obtained by the 2D analysis are slightly lower than the values obtained using the hexahedral and tetrahedral elements.

The value of the stress intensity factor of Mode I after the crack opening displacement obtained in the FRANC2D/L software was 0.2715 MPamm^{0.5}, which is close to the theoretical value of 0.26108 MPamm^{0.5} obtained by formula (1). During crack propagation in the FRANC2D/L software, the value of K_I was continuously increasing and—unlike the plates with hexahedral and tetrahedral elements—in the 18th step there was no sudden jump of the value (Fig. 14). The jump

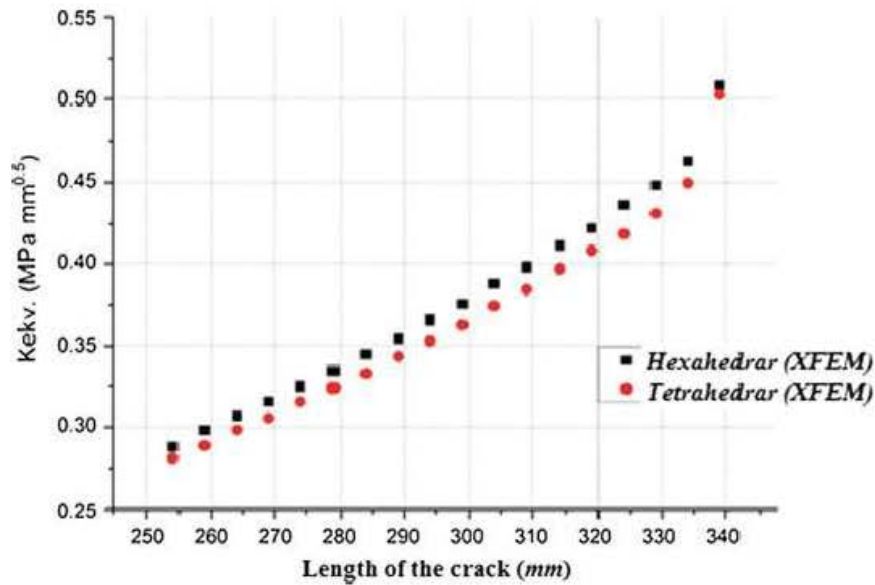


Fig. 13 Graph of variation of the values of equivalent stress intensity factor on the 3D plate with central crack for various types of finite elements

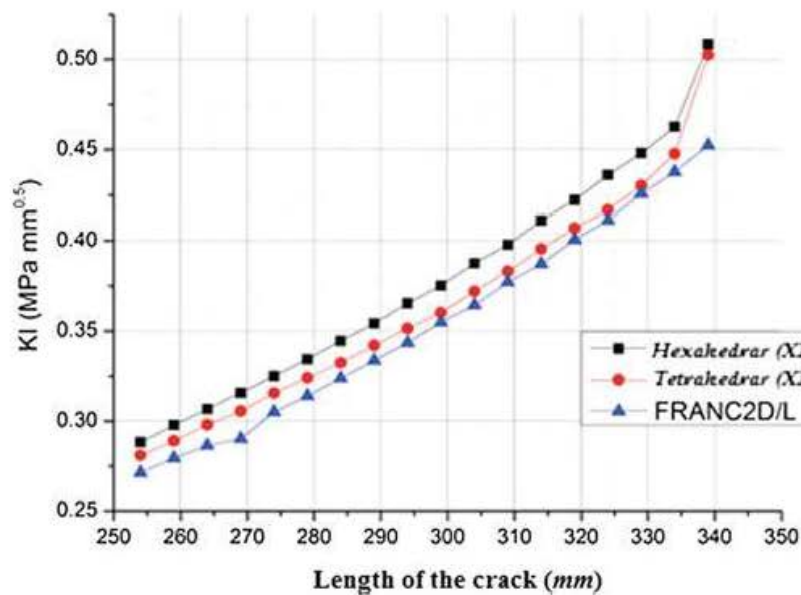


Fig. 14 Graph of variation of the values of stress intensity factor of Mode I on the 3D plate with central crack (hexahedral and tetrahedral elements, Abacus) and 2D plate (FRANC2D/L)

of the value of K_I on the 3D plates is a consequence of the fact that the crack on them has emerged from the area of high density of the mesh, which is another contribution to the thesis that **the quality of the mesh is crucial when the accuracy of the results of simulation is concerned.**

Finally, Table 3 gives a comparative overview of the values of K_I obtained in the FRANC2D/L and Abaqus software on the plate with tetrahedrons, which gave more accurate results than the hexahedron (which is the result of the much larger number

Table 3 Comparative overview of the values of stress intensity factor of Mode I for 3D plate with tetrahedral elements (Abaqus) and 2D plate (FRANC2D/L)

Length of the crack (mm)	FRANC2D/ L	Abaqus 3D, tetrahedral elements	Difference (%)
	K_I (MPa mm ^{0.5})		
254	0.2715	0.2811	3.54
259	0.2795	0.2890	3.41
264	0.2865	0.2980	4.01
269	0.2902	0.3056	5.29
274	0.3050	0.3155	3.45
279	0.3140	0.3240	3.19
284	0.3238	0.3324	2.65
289	0.3337	0.3420	2.50
294	0.3435	0.3515	2.32
299	0.3549	0.3602	1.50
304	0.3644	0.3721	2.10
309	0.3771	0.3831	1.60
314	0.3873	0.3955	2.12
319	0.4006	0.4069	1.58
324	0.4113	0.4167	1.32
329	0.4257	0.4301	1.04
334	0.4376	0.4476	2.30
339	0.4523	0.5025	11.10

of finite elements generated on the tetrahedral plate, too). As one can see in Table 3, the differences in the K_I values in steps are not large (from 1.04 to 5.29%), with the exception of the last step (11.10%) already explained (cracks emerging from the area of higher density of the elements). The values obtained definitely indicate that 3D simulation—if the generated mesh is a quality mesh—can also provide sufficiently good values of the stress intensity factors, which can then be used in determining the number of cycles that will lead to the crack propagation from the initial length to its final size.

The estimation of the number of cycles can also be obtained within Abaqus which, based on calculated values of K_{ekv} per steps and introduced values of Paris coefficient (n), Paris exponent (C) and stress ratio (R), calculates the number of cycles using a modified Paris law on crack propagation, given by the equation.

$$\frac{da}{dN} = \frac{C(\Delta K)^n}{(1-R)(Kc - Kmax)} \quad (2)$$

In the case of a central crack on the plate 508×254 mm, the value of the exponent $n = 2.26$ and coefficient $C = 7.526 \times 10^{-11}$, respectively, corresponding

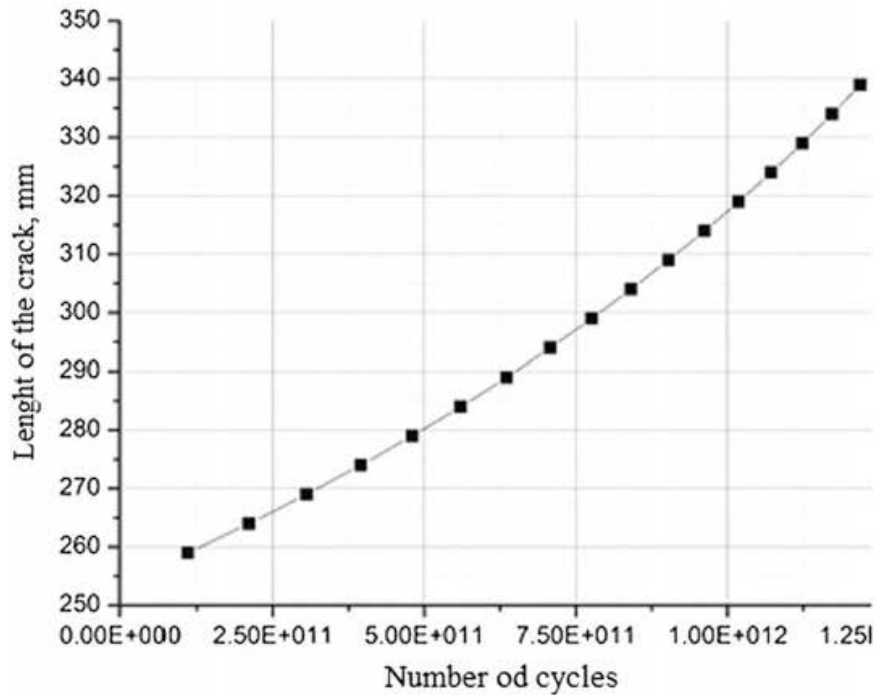


Fig. 15 Graph of variation of the crack length (hexahedral elements, Abaqus) with the number of load cycles

to the steel of HP-9-4-20 190-210 UTS grade were adopted; GTA Weld + SR from NASGRO base. For the ratio of minimum and maximum stress, the value $R = -1$ was adopted.

The graph in Fig. 15 shows that an extremely large number of cycles (order of magnitude 1×10^{11}) is required to make the crack propagate from the initial length of 254 to 259 mm, while for reaching the total length of 339 mm it is necessary to have more than 1.2×10^{12} cycles. This result is not unexpected, because a very low value of tensile stress (only 0.00689 MPa) was used in the calculation.

It is interesting to note that the NASGRO software for an identical model of plate, only of infinite length, showed the message “crack does not propagate” when attempting to make the crack to propagate, and as a result gave the number of cycles equal to zero. This also confirms that the applied load is very low and that under such a load the crack will propagate by a couple of millimeters only after a very large number of cycles.

However, the actual value of the cycle number can only be obtained by fatigue testing.

Conclusions

Over the years, many numerical techniques such as finite element method (FEM), boundary element method (BEM), meshfree methods and extended finite element method (XFEM) have been developed to simulate the fracture mechanics problems. In XFEM, the conformal meshing is not required, hence, the modelling of moving discontinuities or crack growth is performed with an ease.

Numerical calculation using XFEM, such as that presented in this paper, makes it possible to study complex real problems, including a comprehensive parametric analysis of all influential factors. Detailed three-dimensional elastic-plastic models, which consider the corresponding properties of microstructural heterogeneity of ductile materials, as well as various structural solutions of the seam geometry and various forms of cracks, provide the possibility of—for instance—effective testing of heterogeneity of the welded joint, the strain and stress state in critical areas, singularity effects and the determination of the parameters of elasto-plastic mechanics.

The main advantage of XFEM lies in possibility of SIFs values evaluation on complex cracked geometry but—at the same time—XFEM results are mesh sensitive and depend on the mesh density in the fracture process region. Mesh size must be determined carefully to ensure the computational efficiency and accuracy; therefore, experimental verification of FE model is still necessary, particularly when geometry is result of completely innovative design.

Acknowledgements This work is a contribution to the Ministry of Education and Science of the Republic of Serbia funded Project TR 35011.

References

1. Sedmak, A., *Primena mehanike loma na integritet konstrukcija*, Mašinski fakultet, 2003, ISBN 86-7083-473-1.
2. <http://www.3ds.com/products/catia/>.
3. Jovicic G., Zivkovic M., Vulovic S., *Budgetary fracture and fatigue mechanics*, Faculty of Mechanical Engineering, Kragujevac, 2011.
4. Čulafić V. B., *Introduction to fracture mechanics*, Podgorica, 1999.
5. Grbović A., *Research of the fatigue of structural elements built from super alloys*, doctoral dissertation, Belgrade, 2012.